Title: Self-assembled nanoparticles from hyaluronic acid-paclitaxel prodrugs for direct cytosolic delivery and enhanced antitumor activity

Author: Chaoran Xu Wei He Yaqi Lv Chao Qin Lingjia Shen Lifang Yin

PII: S0378-5173(15)30087-9
DOI: http://dx.doi.org/doi:10.1016/j.ijpharm.2015.07.069
Reference: IJP 15073

To appear in: *International Journal of Pharmaceutics*

Received date: 24-5-2015
Revised date: 18-7-2015
Accepted date: 27-7-2015

Please cite this article as: Xu, Chaoran, He, Wei, Lv, Yaqi, Qin, Chao, Shen, Lingjia, Yin, Lifang, Self-assembled nanoparticles from hyaluronic acid-paclitaxel prodrugs for direct cytosolic delivery and enhanced antitumor activity.International Journal of Pharmaceutics http://dx.doi.org/10.1016/j.ijpharm.2015.07.069

Self-assembled nanoparticles from hyaluronic acid-paclitaxel prodrugs for direct cytosolic delivery and enhanced antitumor activity

Chaoran Xu [a,1], Wei He [a,*], Yaqi, Lv [a], Chao Qin [a], Lingjia Shen [b], Lifang Yin [a,*]

[a] *Department of Pharmaceutics, School of Pharmacy, China Pharmaceutical University, Nanjing 210009, PR China*

[b] *National Engineering and Research Center for Target Drugs, Lianyungang, 222047, PR China*

*To whom correspondence should be addressed: He, W and Yin, LF.

Department of Pharmaceutics, School of Pharmacy, China Pharmaceutical University, Nanjing, 210009, PR China. Tel/Fax: +862583271018; E-mail: weihe@cpu.edu.cn (He, W) and lifangyin@hotmail.com (Yin, LF).

Graphical abstract

Abstract

A prodrug-based nanosystem obtained by formulating prodrug and nanotechnology into a system is one of the most promising strategies to enhance drug delivery for disease treatment. Herein, we report a new nanosystem based on HA-PTX conjugates (HA-PTX Ns), which penetrated across cell membranes into cytosol, thus enhancing paclitaxel (PTX) delivery. HA-PTX Ns were successfully obtained based on HA-PTX, and their average particle size was approximately 200 nm. Importantly, unlike other prodrug-based nanosystems, HA-PTX Ns obtained cellular entry without entrapment within the lysosomal-endosomal system by using pathways including clathrin-mediated endocytosis, microtubule-associated internalization, macropinocytosis and cholesterol-dependence. Due to significant accumulation in tumors, HA-PTX Ns had more than a 4-fold decrease in tumor volume on day 14 in contrast with PTX alone. In conclusion, HA-PTX Ns could enter cells, bypass the lysosomal-endosomal system and improve PTX delivery.

Chemical compounds studied in this article

Paclitaxel (PubChem CID: 44155032); Fluorescein isothiocyanate (PubChem CID: 18730); MTT (PubChem CID: 16218671); IR783 (PubChem CID: 46873808); Diphenylphosphinic chloride (PubChem CID: 73910); Adipic acid dihydrazide (PubChem CID: 66117); Succinic anhydride (PubChem CID: 7922); Carbodiimide hydrochloride (PubChem CID: 15908); triethylamine (PubChem CID: 8471); Pyridine (PubChem CID: 1049).

Keywords: self-assembly, nanoparticles, prodrug, paclitaxel, cytosolic delivery, internalization pathway, antitumor activity

1. Introduction

Nanosystems for drug delivery (NsDD) possess great potential to improve the therapeutic effect of active compounds due to advantages such as enhanced solubility and drug stability, small nanoparticle size, the ability to target drugs to the disease site, changes in pharmacokinetics and tissue biodistribution and reduced side effects (Ashley et al., 2011; Cheng et al., 2012; Davis et al., 2008). However, conventional nanocarriers suffer from drawbacks such as poor stability in physiological conditions, a high tendency to recrystallize during storage, low drug-loading efficiency, premature burst release and poor target site accumulation, therefore resulting in limitations of clinical applications (Duhem et al., 2014; Mura et al., 2015; Zhang et al., 2013). Thus, novel NsDD that can overcome these drawbacks are highly desirable.

Prodrug-based NsDD that integrate prodrug strategies and nanotechnology into a system are some of the most promising ways to enhance the delivery of active compounds owing to their advantages including enhanced drug availability in target sites, high drug-loading capacity, noncrystallization upon encapsulation and controlled and prolonged drug release (Fang and Al-Suwayeh, 2012; Luo et al., 2014). Generally, the currently available prodrug-based NsDD can be classified into three categories: (i) prodrug-nanoparticles prepared by formulating the prodrug into the nanocarriers via noncovalent interactions, (ii) small molecular weight prodrug-nanoparticles obtained by self-assembly of active compounds and (iii) NsDD based on amphiphilic polymer-drug conjugates, which are prepared by self-assembling the conjugates into nanoscaled particles. Due to the exceptionally high drug loading and excellent stability under physiological environments, NsDD based on polymer-drug conjugates are more efficient for drug delivery (Cai et al., 2015; Shen et al., 2010).

Paclitaxel (PTX), a highly hydrophobic drug with water-solubility less than 0.24 mg/L, is one of the most commonly used active compounds in clinics for cancer therapy. PTX suppresses microtubule dynamic instability, which is required for cellular division, and induces apoptosis (Li et al., 2015b; Schiff et al., 1979). However, like many other anticancer drugs, its clinical use is greatly limited by its inherent drawbacks including poor solubility, adverse side effects and poor tumor penetration (He et al., 2015b). In order to solubilize PTX, Cremophor EL and dehydrated ethanol have to be added into the product formulation, Taxol. However, the presence of Cremophor EL in Taxol would in turn generate severe side effects, such as allergy, hypersensitivity, and anaphylactic reactions, thus affecting 20−40% of patients and compromising the therapeutic index for PTX. Therefore, the development of a Cremophor EL-free PTX formulation is urgent.

Hyaluronic acid (HA), a naturally occurring biocompatible polyanionic polysaccharide, is an anionic biopolymer made up of alternating disaccharide units of D-glucuronic acid and N-acetyl-d-glucosamine with a β $(1 \rightarrow 4)$ interglycosidic linkage (Yang et al., 2015). Due to its well-tolerated and biocompatible nature, HA has been widely studied for biomedical applications including tissue engineering, drug delivery and molecular imaging (Li et al., 2015a; Martens et al., 2015). Importantly, HA is also utilized as a targeting ligand in drug carriers because it can effectively bind to the CD44 receptor, which is overexpressed in cancer cells (Liu et al., 2011; Zhong et al., 2015), thus achieving active targeting for anticancer drug delivery.

Herein, we reported a new NsDD based on HA-PTX conjugates. Indeed, other groups reported that HA-PTX is active for tumor therapy (Luo et al., 2000); however, few reports indicated that HA-PTX conjugates could form nanoparticles. Here, we demonstrate that HA-PTX conjugates can self-assemble

into nanoparticles in aqueous conditions. Importantly, we demonstrated that HA-PTX Ns bypassed the lysosomal-endosomal system, were well taken up by cancer cells and were located in cytosol and nucleus. To our best knowledge, NsDDS that can obtain cellular entry without entrapment within the lysosomal-endosomal system have not been reported until now. Such a discovery would be beneficial to enlarge the application of based-polymer-drug conjugate nanosystems, severing as carriers for targeting delivery of protein or gene drugs into the cytosol. Such NsDDS also enhanced antitumor activities compared with free PTX, thus achieving active tumor therapeutic targeting without additional modification of other ligands. Using HA-PTX self-assembled nanopartiles is a promising strategy for enhancing PTX delivery for tumor treatment.

2. Methods and materials

2.1. Materials

PTX (99% purity) was obtained from Yew Biotechnology Co. Ltd. (Jiangsu, China). Taxol (marked product of PTX) was from Bristol-Myers Squibb (China) Investment Co., Ltd. (Shanghai, China). IR 783 probe (90% purity), fluorescein isothiocyanate (FITC, 98% purity), hyaluronidase and MTT (98% purity) were purchased from Sigma-Aldrich Co., Ltd. (St. Louis, MO, USA). Hyaluronic acid, n-hydroxy two imide, diphenyl phosphoryl chloride, adipic acid dihydrazide and succinic anhydride were purchased from Aladdin Industrial Inc. (Shanghai, China). The H22 cell line was purchased from Nanjin Key GEN Biotech Co., Ltd. (Nanjing, China). Anhydrous pyridine, carbodiimide hydrochloride (EDC) and triethylamine were from Lingfeng Chemical Reagent Co., Ltd. (Shanghai, China). Fetal bovine serum, HBS, RPMI-1640, Dulbecco's modified Eagle medium and trypsin were obtained from Thermo Fisher Scientific Inc. (Waltham, MA, USA). DAPI and LysoTracker Red were obtained from

Beyotime Institute of Biotechnology (Haimen, China). All of the other chemicals were of analytical reagent grade and were obtained from Sinopharm Chemical Reagent (Shanghai, China).

Male ICR mice (18–22 g) were purchased from the College of Veterinary Medicine at Yangzhou University (License No: SCXK (Su) 2012-0004, Yangzhou, China). The animals used in the experiments received care in compliance with the Principles of Laboratory Animal Care and the Guide for the Care and Use of Laboratory Animals. The experiments followed the protocol approved by the China Pharmaceutical University Institutional Animal Care and Use Committee.

2.2. Preparation of and characterization of HA-PTX Ns

2.2.1. Synthesis of PTX-NHS

The synthesis of n-hydroxy two imide two phenyl phosphate (SDPP) was performed as described below. In brief, 230 mg n-hydroxy two imide, 34 μL diphenyl phosphoryl chloride and 280 μL triethylamine were added into dichloromethane in order, the mixture was stirred for 12 h under room temperature, and the reaction mixture was placed into a mortar and ground with ethyl ether. Subsequently, the deposition was dissolved with acetic ether and washed with water and saturated sodium chloride solution. Finally, the organic phase was mixed with anhydrous sodium and dried under reduced pressure.

The synthesis of PTX-semi succinyl salt (PTX-semi) was performed as described below. Briefly, 540 mg PTX and 76 mg succinic anhydride were dissolved in dichloromethane. Upon addition of 513 μL anhydrous pyridine, the reaction mixture was stirred for three days at room temperature. After concentration under vacuum conditions, the sample was purified with column chromatography using

acetic ether and n-hexane (1:1, v/v) as eluents.

The synthesis of PTX-NHS was next. After dissolving 300 mg PTX-semi and 164 mg SDPP in acetonitrile, the reaction mixture was mixed with 176 μL triethylamine and stirred at room temperature for 24 h. Upon condensation under vacuum conditions, the mixture was separated with a mixture of acetic ether and n-hexane (1:1, v/v) as eluents (Greenwald et al., 1996).

2.2.2. Synthesis of HA-adipic acid dihydrazide (HA-ADH)

Low molecular weight (MW) HA was prepared as follows: 2 g high MW HA (1.5 MDa) was first dissolved in PBS (pH 6.5, 4 mg/mL), and then hyaluronidase (10 UI/mg) was added into the enzymatic reaction solution, which was kept at 37 ˚C for 1 h and stopped at 90 ˚C. After that, the sample was purified by dialyzing with a dialysis bag (MWCO = 3500 Da) and filtering through a 0.22-μm cellulose acetate membrane. Finally, the purified sample was freeze-dried for use.

HA-ADH synthesis is listed below. ADH (52 mg) was placed into 15 mL low MW HA solution (3 mg/mL), and the reaction mixture was adjusted to pH 4.75 with 0.1 M HCl. It was then blended with 12 mg EDC and reacted for 24 h at pH 4.75. The reaction was stopped by pH regulation to 7.0 with 0.1 M sodium hydroxide. The sample was dialyzed successively against 0.1 M sodium hydroxide, 25% ethanol/water and water (MW cut off 3.5 kDa). The purified sample was finally filtered through a 0.22-μm cellulose acetate membrane and freeze-dried.

2.2.3. Synthesis of HA-PTX conjugation

Thirty milliliters of 1 mg/mL HA-ADH in PBS was mixed with 2:1 (v/v) DMF/water containing 8 mg PTX-NHS, and then the mixture was stirred for 24 h at room temperature. Subsequently, the reaction

mixture was paced into a dialysis bag (MWCO = 3500 Da) and dialyzed against 25% ethanol/water and water. After filtration through a 0.22-μm membrane, the sample was freeze-dried (Luo et al., 2000). The final activated conjugation and all of the intermediates were characterized by UV, IR and NMR spectroscopy.

2.2.4. Preparation and characterization of HA-PTX Ns

Five milligrams HA-PTX conjugation was dispersed in 5 mL water, and the solution was sonicated for 10 min with probe ultrasonication (20–25 kHz, Ningbo Scientz Biotechnology Co. Ltd., China) at 100 W. The ultrasound pulse was turned off for 3 s with a period of 3 s. During the process, the temperature was controlled by placing the sample in an ice-water bath. The final HA-PTX Ns was obtained by filtering the sample through a 0.22-μm membrane.

Particle size and polydispersity index (PI) were determined with a 90Plus Particle Size Analyzer (Brookhaven Instruments, Holtsville, NY) at room temperature based on the DLS principle. Raw data were obtained over 5 min at an angle of 90°. The diameter of HA-PTX Ns was expressed with intensity-weighted Gaussian distribution (with Chi-squared value <3).

HA-PTX Ns morphology was examined with TEM (JEM-1230, Tokyo, Japan) at an acceleration voltage of 200 kV. In total, one drop of sample was placed on a copper mesh and dried at 25 ℃ after removing the excessive sample with filter paper, and one drop of 2% (w/w) phosphotungstic acid was then deposited on the copper and left for 1 min. After removing the extra phosphotungstic acid, the copper was dried at room temperature for 10 min.

2.3. Cellular uptake and internalization pathway

H22 cells were seeded on 24-well plates at a density of 1×10^4 cells/well and cultured for 24 h at 37 °C. Then, the cells were incubated with FITC labeled HA-PTX Ns (FITC-HA-PTX Ns) or PTX (FITC-PTX) for 4 h at various FITC concentrations at 37 °C or 4 °C. At the end of the experiment, the cells were washed three times with PBS, and the florescence intensity was measured with flow cytometry (BD FACSCalibur, USA).

H22 cells were seeded on 6-well plates at a density of 1×10^5 cells/well and cultured for 24 h at 37 °C. The culture medium was then replaced with fresh medium, which contained endocytotic pathway inhibitors including cytochalasin-D (10 μg/mL), nystatin (10 μM), chlorpromazine (10 μg/mL), nocodazole (20 μM), methyl-β-cyclodextrin (M-β-CD, 2.5 mM), monensin (200 nM) and NaN_3 (10 mM) + deoxyglucose (DG, 50 mM). After treatment with the inhibitors for 30 min at 37 °C, the cells were incubated with FITC-HA-PTX Ns for 4 h, in which the FITC concentration in each well was 2 μg/mL. Cellular fluorescence intensity was determined using flow cytometry after trypsinization.

2.4. Intracellular location

H22 cells were seeded on a 30-mm cell culture dish with a glass bottom at a density of 1×10^5 cells/dish and cultured for 24 h. The cells were then treated with FITC-HA-PTX Ns or FITC-PTX for 4 h (2 μg/mL FITC in PBS). Subsequently, 1 μL Lyso-Tracker Red was added, and the cells were incubated for 2 h, washed three times with PBS and stained with DAPI for 15 min. The cells were examined using CLSM (LECIA TCS SP5 II, Heidelberg, Germany).

2.5. In vitro cytotoxicity

To assess the cytotoxicity, the cell viabilities against HA and HA-ADH without PTX were studied. H22 cells were seeded on 96-well plates at a density of 5×10^3 cells/well and cultured for 24 h. The cells were then incubated with HA and HA-ADH at various concentrations. Cell viability was evaluated using an MTT assay.

2.6. Cell apoptosis assay

H22 cells were seeded on 12-well plates at a density of 1×10^5 cells/well and cultured for 24 h. The cells were then incubated with HA-PTX Ns, Taxol or saline for 72 h at a PTX concentration of 1, 000 ng/mL. The cell apoptosis was detected with an FCM analysis using an Annexin V-FITC/PI apoptosis detection kit (Bender Medsystems, Vienna, Austria).

2.7. In vivo imaging

H22 tumor-bearing mice were prepared as follows: 0.2 mL cell suspension at a density of 1×10^7 cells/mL was injected subcutaneously into the scapula region of the mice. Treatment began as the tumor size reached a volume of $10\times10\times5$ mm^3.

The mice were anesthetized with a 4% novochlorhydrate solution, and fluorescence images were taken with an in vivo imaging system (In-Vivo FX PRO, Carestream, Canada) at 1, 2 and 4 h after intravenous administration of 0.5 mg/kg IR783 via the tail vein.

2.8. Antitumor activity

H22 tumor-bearing mice were randomly divided into three groups (9 mice per group): saline, Taxol and HA-PTX Ns. Mice were injected intravenously via the tail vein at a dose of 20 mg/kg of PTX based on body weight. At predetermined time points, tumor volume was measured.

2.9. Statistical Analysis

The data are expressed as the mean ±standard deviation, and differences were considered to be statistically significant when the P value was less than 0.05.

3. Results

3.1. Synthesis of HA-PTX

The HA-PTX preparation method is presented in Fig. 1. Two intermediates (PTX-NHS and HA-ADH) were first obtained. PTX-NHS was synthesized by linking NHS to C2'-hydroxyl groups of PTX via substitution and esterification reactions while HA-ADH was prepared through grafting free amino groups of ADH to HA with EDC as a condensation agent. Subsequently, HA-PTX conjugates were obtained via a nucleophilic reaction between free HA and PTX-NHS amino groups. The chemical structures of intermediates and HA-PTX conjugates were confirmed using ^{1}H NMR, UV and IR spectroscopy (Figs. 2 and 3). As demonstrated in Fig. 2 (A and B), the dd split peaked at the methylene proton at 2.33 and 2.12 ppm from succinimide and succinic acid, respectively, as indicated by PTX-NHS formation, whereas the methylene proton signals at 1.3–1.4 ppm, suggesting grafting of ADH to HA. However, in the ^{1}H NMR spectra of HA-PTX (Fig. 2C), the characteristic peaks were not observed, which might be because its MW was too high. Thus, the UV vis spectra were further used to

confirm HA-PTX structure. As depicted in Fig. 2(D), the characteristic peaks at 200 and 230 nm that belonged to HA and PTX (Pouyani and Prestwich, 1994), respectively, were observed, therefore demonstrating the presence of PTX and HA in the conjugations. HA-PTX, HA-ADH and PTX-NHS formation was also verified by IR spectra. For PTX-NHS, there were two activated carbonyl groups, which made two characteristic peaks appear at 1750–1850 cm^{-1}. As indicated in Fig. 3(A), two absorption peaks located at 1786.2 and 1818.1 cm^{-1} indicating SDPP were linked to PTX (Li et al., 2011). In contrast, characteristic peaks for the carbonyl groups did not appear in HA-PTX with a characteristic absorption related to HA at approximately 3500 cm^{-1}, while other absorption peaks exhibited as a simple superimposition of HA-ADH and PTX-NHS, therefore confirming the formation of HA-PTX (Fig. 3 (B and C)). Calculating by the equation of PTX loading (%) = amount of PTX in conjugation/amount of PTX addition × 100%, the drug loading in HA-PTX Ns was approximately 47.2%.

3.2. Preparation and Characterization of HA-PTX Ns

The procedure for HA-PTX Ns preparation is depicted in Fig. 1. HA-PTX Ns were prepared by dispersing HA-PTX conjugations into aqueous solution followed by ultrasonication. The size in HA-PTX Ns diameter as determined by the DLS principle was approximately 200 nm with a PI value less than 0.3 (Fig. 4A), which thus suggested a narrow size distribution (He et al., 2013). To examine the morphology and further confirm the particle size of HA-PTX Ns, TEM observation was performed. As demonstrated in Fig. 4(B), spherical particles are displayed that have a diameter of 50–80 nm without any aggregation. The smaller size, in contrast with the DLS data, might be because of the procedure that was used for the TEM test sample preparation. The nanoparticle size during TEM

analysis would become smaller because of the high energy of the electron beam and thus production of local heating in the particles (Blasi et al., 2011).

3.3. Cellular uptake and internalization pathway

The uptake of FITC labeled HA-PTX Ns or PTX in H22 cells at 37 ℃ or 4 ℃ is displayed in Fig. 5 (A). HA-PTX Ns or PTX uptake generally increased with an increase in the amount of the two PTX formulations, indicating that uptake was concentration-dependent. Importantly, the fluorescence intensity of FITC-HA-PTX Ns, despite of FITC concentrations and temperature, was significantly higher than FITC-PTX, therefore indicating enhanced cellular uptake from the former. Interestingly, irrespective of concentrations, considerable HA-PTX Ns uptake was also observed at 4 ℃, which indicated that HA-PTX Ns were taken up following a nonendocytic mechanism (He et al., 2015a; Hillaireau and Couvreur, 2009).

To study internalization mechanisms，HA-PTX Ns uptake was assessed in H22 cells that had been pretreated with inhibitors. Inhibitors such as CPZ, Cyto-D, nystatin, nocodazole, monensin, M-CD, BFA and NaN_3 with DG (NaN_3+DG), which inhibited clathrin-mediated endocytosis, macropinocytosis, caveolin-mediated internalization, microtubule-related internalization, lysosome-involved internalization, cholesterol-dependence, Golgi apparatus-related internalization and energy-dependent mechanisms, respectively, were involved in the experiment. As displayed in Fig. 5 (B), the fluorescence intensity was reduced significantly by several inhibitors including CPZ, monensin, nystatin and M-CD. These data thus indicated that cellular uptake was controlled by more than one pathway, which included clathrin-mediated endocytosis, microtubule-associated internalization, macropinocytosis and cholesterol-dependence.

3.4. In vitro cytotoxicity and cell apoptosis

To assess HA-PTX Ns cytotoxicity, cells were cultured with HA and HA-ADH without PTX for 24 h at 37 °C. As demonstrated in Fig. 6 (A), cell viability was greater than 90% irrespective of the concentrations, thus indicating better compatibility.

An Annexin V-FITC/PI kit was used to stain the early and late apoptotic cells, and the percentage of apoptotic cells was measured using FCM. The total percentage of apoptosis in H22 cells was 15.0%, 2.8% and 0.68% for HA-PTX Ns, Taxol and saline (Fig. 6B), respectively, thereby indicating that HA-PTX Ns was most efficient in inducing apoptosis in cancer cells.

3.5. Intracellular location

To examine the intracellular localization of FITC-labeled HA-PTX Ns following their internalization, the cellular distribution of FITC-HA-PTX Ns was determined by CLSM. As demonstrated in Fig. 7(A), green fluorescence was observed throughout the cytosol and nucleus. In contrast, lysosomal staining of the cells that had been treated with FITC-HA-PTX Ns did not display lysosomal localization of HA-PTX Ns (Fig. 7B). These results thus confirmed that the cellular uptake of HA-PTX was not involved in the lysosomal-endosomal system

3.6. In vivo imaging

To examine its tumor-targeting capacity, in vivo fluorescence imaging was performed in tumor-bearing mice that had been injected with IR783-HA-PTX Ns at 1, 2 and 4 h post-administration. As demonstrated in Fig. 8, strong fluorescence intensity in tumors was observed, with increased intensity within 1 to 4 h after injection, therefore demonstrating significant HA-PTX Ns accumulation in tumors.

Indeed, besides the target tissue, HA-PTX Ns were also distributed into other tissues such as the liver and brain.

3.7. Antitumor activity

PTX formulations, Taxol and HA-PTX Ns, were injected intravenously into H22 tumor-bearing mice via the tail vein using saline as a control. Tumor volumes for each group were recorded, and the change in tumor volume was calculated every three days to evaluate antitumor activity. The time versus tumor volume is present in Fig. 9. Tumor volume in the saline group increased rapidly without any inhibition of tumor growth. Tumor growth from the Taxol-injected group (a marked product) was significantly suppressed after 14 days of administration. In contrast, tumor growth from the HA-PTX Ns-treated group was slowed dramatically, and the tumor volume at each time point was markedly reduced, leading to more than a 4- and 5-fold decrease on day 14 compared with Taxol and saline, respectively, therefore indicating a significant improvement in antitumor activity.

4. Discussion

The HA-PTX conjugations could self-assemble into nanoparticles with a particle size of approximately 200 nm. HA-PTX conjugations were synthesized by coupling hydrophobic PTX-NHS molecules to the hydrophilic HA with an esterification reaction. Due to the presence of a number of active groups (–COOH) in the HA structural skeleton, a considerable amount of PTX molecules would be readily grafted onto the polymer, forming a comb-like copolymer prodrug and resulting in a high drug payload (Li et al., 2011; Luo et al., 2014). Importantly, the HA-PTX conjugations, which have hydrophobic moieties and a hydrophilic skeleton and thus have an amphiphilic nature, can act as an amphiphilic

material and therefore self-assemble into supramolecular nanostructures in aqueous conditions via noncovalent interactions. Such supramolecular nanostructures were based on HA-PTX conjugations, which would facilitate PTX delivery because of advantages of the nanoparticle drug delivery system, thereby allowing enhanced cancer therapy.

We have demonstrated that HA-PTX Ns were taken up well by cancer cells and were located in the cytosol and nucleus without detainment by the lysosomal-endosomal system. It was evident that a large amount of HA-PTX Ns obtained cellular uptake at 4 °C (Fig. 5A). Because of membrane fluidity inhibition at low temperature, nanoformulation accumulation in cells can only rely on direct penetration across the membrane into the cytosol (Lee et al., 2012). Moreover, the lysosomal staining of cells that had been incubated with FITC-HA-PTX Ns did not exhibit the colocalization of FITC signals with LysoTracker (Fig. 7B) therefore further confirming its cellular entry via penetration across the membrane. It might be related to the hydrophobic area from the hydrophobic PTX with a relatively high MW onto the surface of supramolecular nanostructures. Previous reports indicated that the presence of specific hydrophobic content on the surface of nanomedicines such as protein-coated nanoparticles and carbon nanotubes could help the nanomedicines obtain direct cytosol delivery via cholesterol or lipid rafts from the interaction between the hydrophobic site and the cell membrane (He et al., 2015a; Verma et al., 2008). As displayed in Fig. 5(B), the cholesterol-dependence pathway was involved in the cellular uptake of HA-PTX Ns, which partly supports our speculation. Nevertheless, more experiments should be performed to elucidate how the nanoparticles obtained cytosolic delivery.

HA-PTX Ns had a significant enhancement in antitumor activity compared with Taxol, which resulted from a combination of passive and active targeting mechanisms. First, HA reportedly acted as a

targeting moiety that can specifically bind to the CD44 receptor, which is highly expressed in cancer cells, thus allowing HA-conjugated nanoparticles or prodrugs to obtain enhanced cellular uptake and cytotoxicity (Oh et al., 2010; Zhong et al., 2015). The uptake was confirmed by cellular uptake assays and in vivo imaging. As depicted in Fig. 5(A), cellular accumulation of HA-PTX Ns was markedly higher than PTX alone, irrespective of the drug concentrations. As well known, there are considerable amounts of esterases in the cell cytosol and lysosomes (Zhang etal., 2013). Thus, Once HA-PTX Ns enter the cells, the ester linkage in HA-PTX conjugations will be easily broken after exposure to intracellular esterase, thereby leading to release of free PTX. A significant accumulation of HA-PTX Ns in tumors was observed from the in vivo image performance (Fig. 8). The percentage of apoptosis in H22 cells induced by HA-PTX Ns was 5-fold as great as that of Taxol (Fig. 6B). Second, nanosized HA-PTX Ns facilitated the improved antitumor activity because they promoted penetration into the tumor interstitium via leaky vasculature (Petros and DeSimone, 2010; Rodriguez et al., 2013). Indeed, more experiments such as pharmacokinetics, biodistribution and biocompatibility should be performed to study the in vivo performance of HA-PTX Ns and confirm their targeting mechanisms.

5. Conclusions

In this study, supramolecular nanostructures of approximately 200 nm in diameter based on the self-assembly of HA-PTX conjugations in aqueous conditions were successfully obtained. Importantly, HA-PTX Ns obtained cytosolic delivery via bypassing the lysosomal-endosomal system, which was dependent on more than one internalization pathway. Few reports indicate that the nanosystems, when self-assembled from polymer-drug conjugates, can penetrate across the cell membrane directly. Such a discovery would help broaden the application of based-polymer-drug conjugate nanosystems, which

serve as carriers for biological macromolecular drugs that need to rapidly escape from the lysosomal-endosomal system into the cytosol. As expected, HA-PTX Ns displayed a significant enhancement in antitumor activity compared with Taxol owing to a combination of passive and active targeting mechanisms. In conclusion, HA-PTX Ns can directly translocate across the membrane into cytosol and is a promising strategy for enhancing PTX delivery for tumor treatment.

Acknowledgments

This study was supported by the National Natural Science Foundation of China (No. 81402869 and No. 81473152), the Natural Science Foundation of the Jiangsu Province (No. BK20140671), the Fostering Plan of University Scientific and Technological Innovation Team of Jiangsu Qing LanProject (2014) and the Creation of Major New Drugs National Major Projects (2014ZX09507004-001, 2014ZX09507004-002).

References

Ashley, C.E., Carnes, E.C., Phillips, G.K., Padilla, D., Durfee, P.N., Brown, P.A., Hanna, T.N., Liu, J., Phillips, B., Carter, M.B., Carroll, N.J., Jiang, X., Dunphy, D.R., Willman, C.L., Petsev, D.N., Evans, D.G., Parikh, A.N., Chackerian, B., Wharton, W., Peabody, D.S., Brinker, C.J., 2011. The targeted delivery of multicomponent cargos to cancer cells by nanoporous particle-supported lipid bilayers. Nature Materials 10, 389–397.

Blasi, P., Giovagnoli, S., Schoubben, A., Puglia, C., Bonina, F., Rossi, C., Ricci, M., 2011. Lipid nanoparticles for brain targeting I. Formulation optimization. International Journal of Pharmaceutics 419, 287–295.

Cai, K., He, X., Song, Z., Yin, Q., Zhang, Y., Uckun, F.M., Jiang, C., Cheng, J., 2015. Dimeric drug polymeric nanoparticles with exceptionally high drug loading and quantitative loading efficiency. Journal of the American Chemical Society 137, 3458–3461.

Cheng, Z., Al Zaki, A., Hui, J.Z., Muzykantov, V.R., Tsourkas, A., 2012. Multifunctional nanoparticles: cost versus benefit of adding targeting and imaging capabilities. Science 338, 903–910.

Davis, M.E., Chen, Z., Shin, D.M., 2008. Nanoparticle therapeutics: an emerging treatment modality for cancer. Nature Review Drug Discovery 7, 771–782.

Duhem, N., Danhier, F., Pourcelle, V., Schumers, J.M., Bertrand, O., Leduff, C.S., Hoeppener, S., Schubert, U.S., Gohy, J.F., Marchand-Brynaert, J., Preat, V., 2014. Self-assembling doxorubicin-tocopherol succinate prodrug as a new drug delivery system: synthesis, characterization, and in vitro and in vivo anticancer activity. Bioconjugate Chemistry 25, 72–81.

Fang, J.-Y., Al-Suwayeh, S.A., 2012. Nanoparticles as delivery carriers for anticancer prodrugs. Expert

Opinion on Drug Delivery 9, 657–669.

Greenwald, R.B., Gilbert, C.W., Pendri, A., Conover, C.D., Xia, J., Martinez, A., 1996. Drug delivery systems: water soluble taxol 2‘-poly(ethylene glycol) ester prodrugsdesign and in vivo effectiveness. Journal of Medicinal Chemistry 39, 424–431.

He, W., Jin, Z., Lv, Y., Cao, H., Yao, J., Zhou, J., Yin, L., 2015a. Shell-crosslinked hybrid nanoparticles for direct cytosolic delivery for tumor therapy. International Journal of Pharmaceutics 478, 762–772.

He, W., Lu, Y., Qi, J., Chen, L., Hu, F., Wu, W., 2013. Nanoemulsion–templated shell-crosslinked nanocapsules as drug delivery systems. International Journal of Pharmaceutics 445, 69–78.

He, W., Lv, Y., Zhao, Y., Xu, C., Jin, Z., Qin, C., Yin, L., 2015b. Core–shell structured gel-nanocarriers for sustained drug release and enhanced antitumor effect. International Journal of Pharmaceutics 484, 163–171.

Hillaireau, H., Couvreur, P., 2009. Nanocarriers' entry into the cell: relevance to drug delivery. Cellular and Molecular Life Sciences: CMLS 66, 2873–2896.

Lee, J., Sharei, A., Sim, W.Y., Adamo, A., Langer, R., Jensen, K.F., Bawendi, M.G., 2012. Nonendocytic delivery of functional engineered nanoparticles into the cytoplasm of live cells using a novel, high-throughput microfluidic device. Nano Letters 12, 6322–6327.

Li, G.L., Liu, J.Y., Pang, Y., Wang, R.B., Mao, L.M., Yan, D.Y., Zhu, X.Y., Sun, J., 2011. Polymeric micelles with water-insoluble drug as hydrophobic moiety for drug delivery. Biomacromolecules 12, 2016–2026.

Li, J., Yin, T., Wang, L., Yin, L., Zhou, J., Huo, M., 2015a. Biological evaluation of redox-sensitive micelles based on hyaluronic acid-deoxycholic acid conjugates for tumor-specific delivery of paclitaxel.

International Journal of Pharmaceutics 483, 38–48.

Li, Y., Wu, Z., He, W., Qin, C., Yao, J., Zhou, J., Yin, L., 2015b. Globular protein-coated paclitaxel nanosuspensions: interaction mechanism, direct cytosolic delivery, and significant improvement in pharmacokinetics. Molecular Pharmaceutics 12, 1485–1500.

Liu, Y., Sun, J., Cao, W., Yang, J., Lian, H., Li, X., Sun, Y., Wang, Y., Wang, S., He, Z., 2011. Dual targeting folate-conjugated hyaluronic acid polymeric micelles for paclitaxel delivery. International Journal of Pharmaceutics 421, 160–169.

Luo, C., Sun, J., Sun, B., He, Z., 2014. Prodrug-based nanoparticulate drug delivery strategies for cancer therapy. Trends in Pharmacological Sciences 35, 556–566.

Luo, Y., Ziebell, M.R., Prestwich, G.D., 2000. A hyaluronic acid−taxol antitumor bioconjugate targeted to cancer cells. Biomacromolecules 1, 208–218.

Martens, T.F., Remaut, K., Deschout, H., Engbersen, J.F.J., Hennink, W.E., van Steenbergen, M.J., Demeester, J., De Smedt, S.C., Braeckmans, K., 2015. Coating nanocarriers with hyaluronic acid facilitates intravitreal drug delivery for retinal gene therapy. Journal of Controlled Release 202, 83–92.

Mura, S., Bui, D.T., Couvreur, P., Nicolas, J., 2015. Lipid prodrug nanocarriers in cancer therapy. Journal of Controlled Release. 208, 25–41.

Oh, E.J., Park, K., Kim, K.S., Kim, J., Yang, J.-A., Kong, J.-H., Lee, M.Y., Hoffman, A.S., Hahn, S.K., 2010. Target specific and long-acting delivery of protein, peptide, and nucleotide therapeutics using hyaluronic acid derivatives. Journal of Controlled Release 141, 2–12.

Petros, R.A., DeSimone, J.M., 2010. Strategies in the design of nanoparticles for therapeutic applications. Nature Review Drug Discovery 9, 615–627.

Pouyani, T., Prestwich, G.D., 1994. Functionalized derivatives of hyaluronic-acid oligosaccharides - drug carriers and novel biomaterials. Bioconjugate Chemistry 5, 339–347.

Rodriguez, P.L., Harada, T., Christian, D.A., Pantano, D.A., Tsai, R.K., Discher, D.E., 2013. Minimal "Self" peptides that inhibit phagocytic clearance and enhance delivery of nanoparticles. Science 339, 971–975.

Schiff, P.B., Fant, J., Horwitz, S.B., 1979. Promotion of microtubule assembly in vitro by taxol. Nature 277, 665–667.

Shen, Y., Jin, E., Zhang, B., Murphy, C.J., Sui, M., Zhao, J., Wang, J., Tang, J., Fan, M., Van Kirk, E., Murdoch, W.J., 2010. Prodrugs forming high drug loading multifunctional nanocapsules for intracellular cancer drug delivery. Journal of the American Chemical Society 132, 4259–4265.

Verma, A., Uzun, O., Hu, Y., Hu, Y., Han, H.S., Watson, N., Chen, S., Irvine, D.J., Stellacci, F., 2008. Surface-structure-regulated cell-membrane penetration by monolayer-protected nanoparticles. Nature Materials 7, 588–595.

Yang, C., Wang, X., Yao, X., Zhang, Y., Wu, W., Jiang, X., 2015. Hyaluronic acid nanogels with enzyme-sensitive cross-linking group for drug delivery. Journal of Controlled Release 205, 206–217.

Zhang, H., Wang, J., Mao, W., Huang, J., Wu, X., Shen, Y., Sui, M., 2013. Novel SN38 conjugate-forming nanoparticles as anticancer prodrug: in vitro and in vivo studies. Journal of Controlled Release 166, 147–158.

Zhong, Y., Zhang, J., Cheng, R., Deng, C., Meng, F., Xie, F., Zhong, Z., 2015. Reversibly crosslinked hyaluronic acid nanoparticles for active targeting and intelligent delivery of doxorubicin to drug resistant CD44+ human breast tumor xenografts. Journal of Controlled Release 205, 144–154.

Figure captions

Fig. 1. Flow chart of the procedure for HA-PTX conjugations and preparation of HA-PTX Ns.

Fig. 2. ^{1}H-NMR spectra of (A) PTX-NHS, (B) HA-ADH and (C) HA-PTX; Ultraviolet spectrum of (A) HA-PTX.

Fig. 3. Infrared spectra of (A) PTX-NHS, (B) HA-ADH and (C) HA-PTX.

Fig. 4. Characterization of HA-PTX Ns. (A) Particle size and distribution. (B) TEM picture. The scale bar is 100 nm.

Fig. 5. (A) Uptake of PTX and FITC-HA-PTX Ns with different FITC concentrations in H22 cells at 4 or 37 ˚C. * represents $p<0.01$.

(B) Endocytic mechanism of HA-PTX Ns in H22 cells. The cells were incubated with FITC labeled HA-PTX Ns (100 ng/mL) for 2 h in the presence of various inhibitors. * represents $p<0.05$. (n=5).

Fig. 6. (A) In vitro cytotoxicity of HA and HA-ADH (n=5). **(B)** H22 cell apoptosis induced by HA-PTX Ns and Taxol, which saline was used as control.

Fig. 7. Location of FITC-labeled HA-PTX Ns in H22 cells that had been treated with PTX formulations containing 2 μg/mL FITC for 4 h. **(A)** Nuclei (blue area) were stained with DAPI. **(B)** Lysosomes (red area) were stained with LysoTracker Red.

Fig. 8. In vivo imaging of H22 tumor-bearing mice that had been injected with IR783 labeled HA-PTX Ns at 1, 2 and 4 h. Each mouse was injected with IR783 labeled HA-PTX Ns at a dose of 200 ng IR783.

Fig. 9. Tumor growth inhibition of free PTX and HA-PTX Ns using saline as a control, *, ** and *** indicate $p<0.05$, $p<0.01$ and $p<0.001$, respectively.

Figure 1

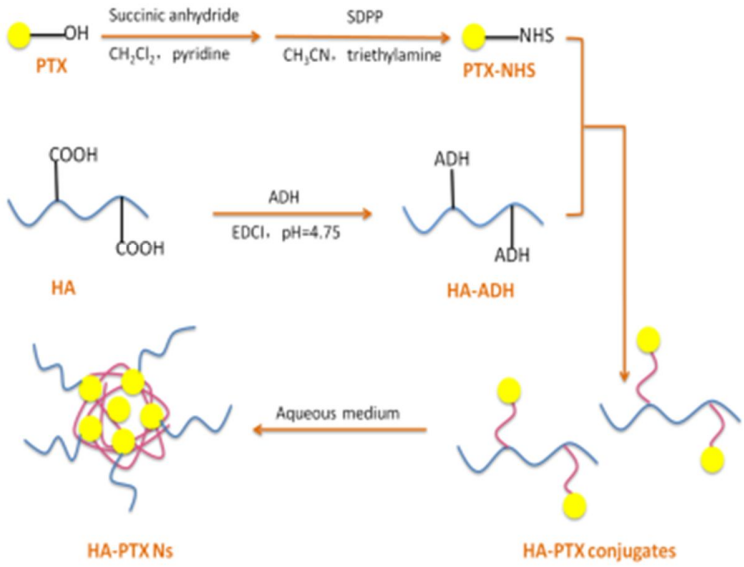

Figure 2

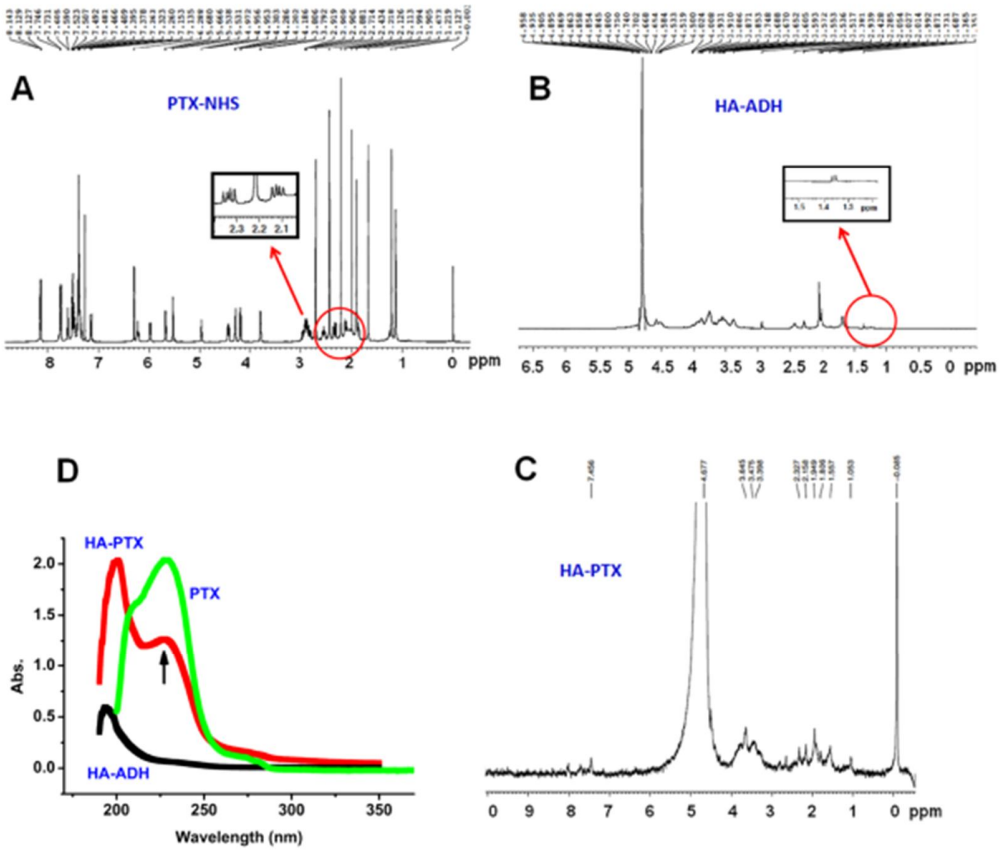

Figure 3

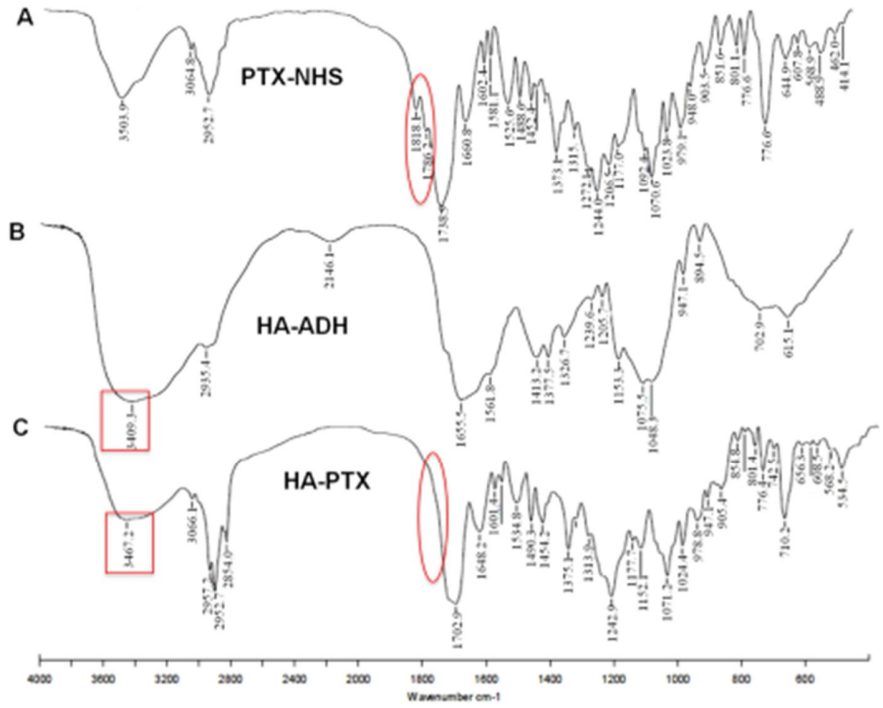

Figure 4

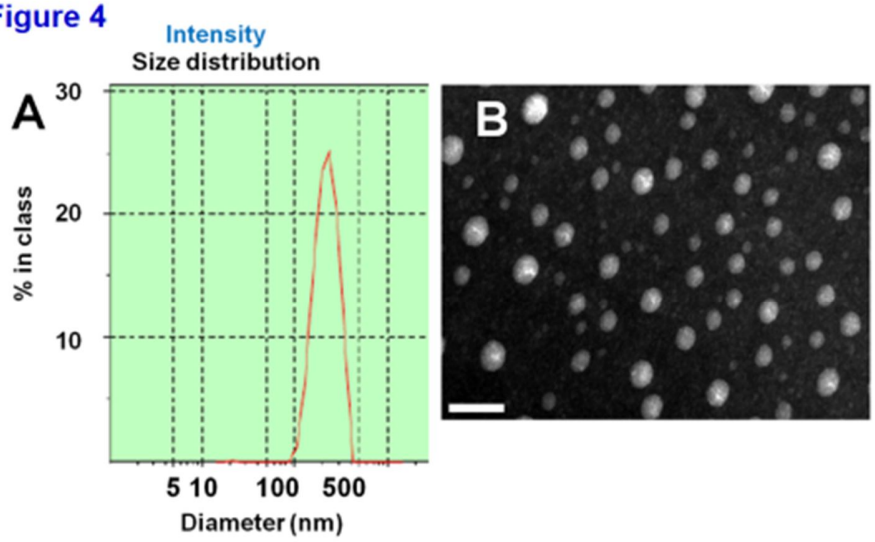

Figure 5

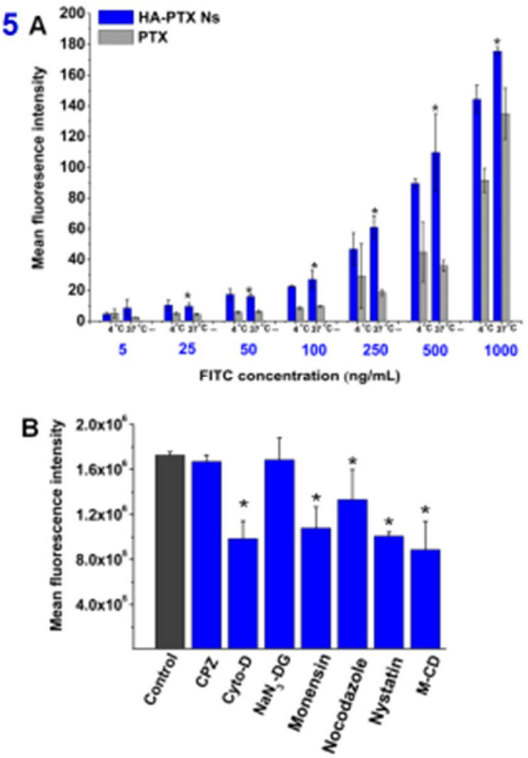

Figure 6

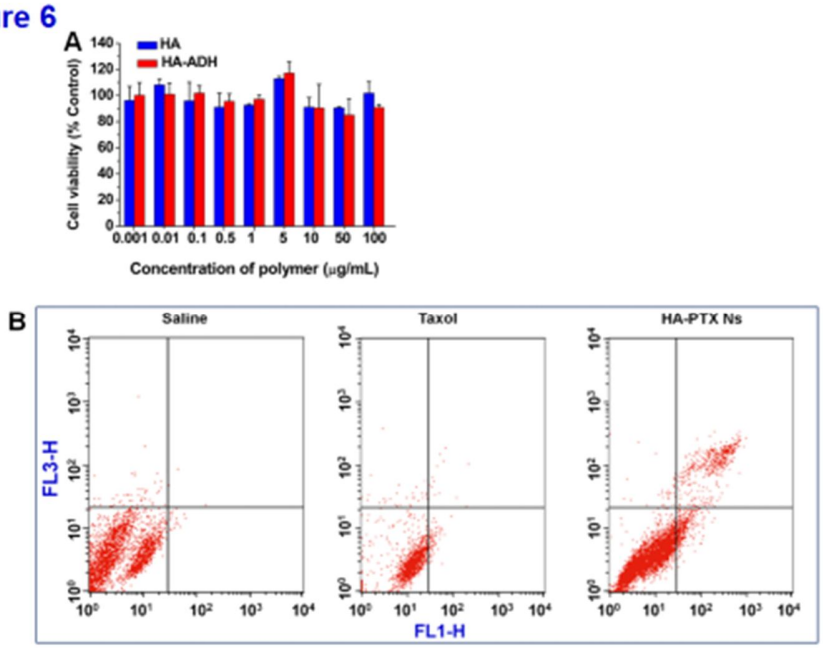

Figure 7

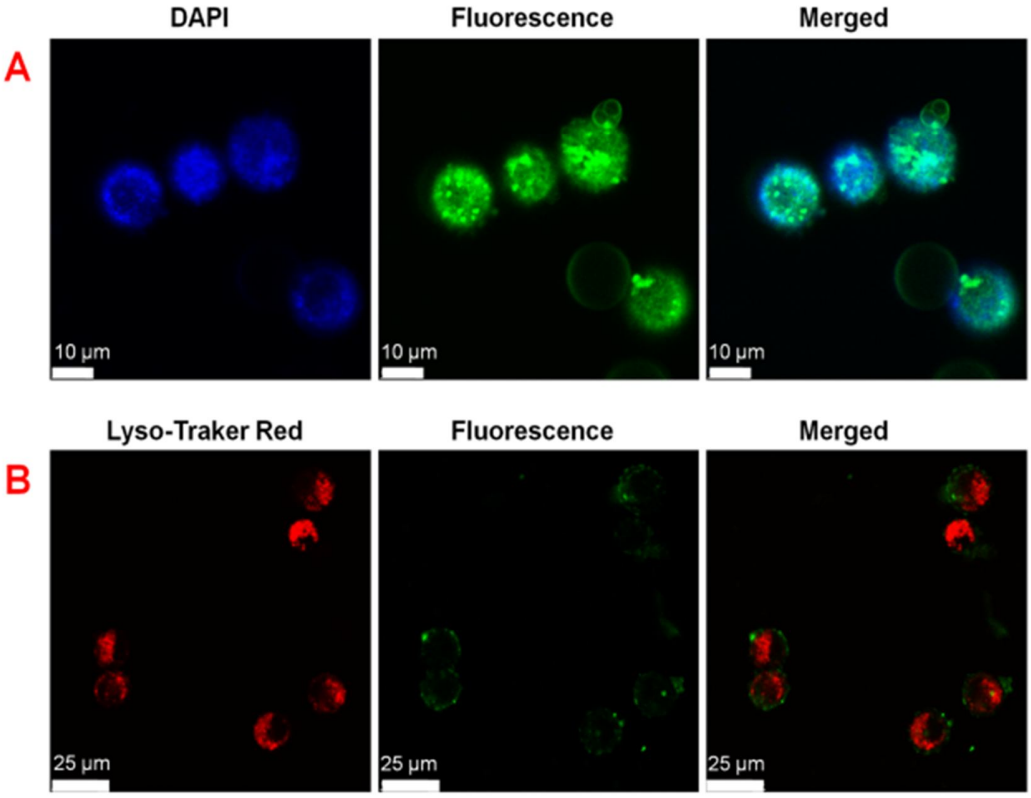

Figure 8

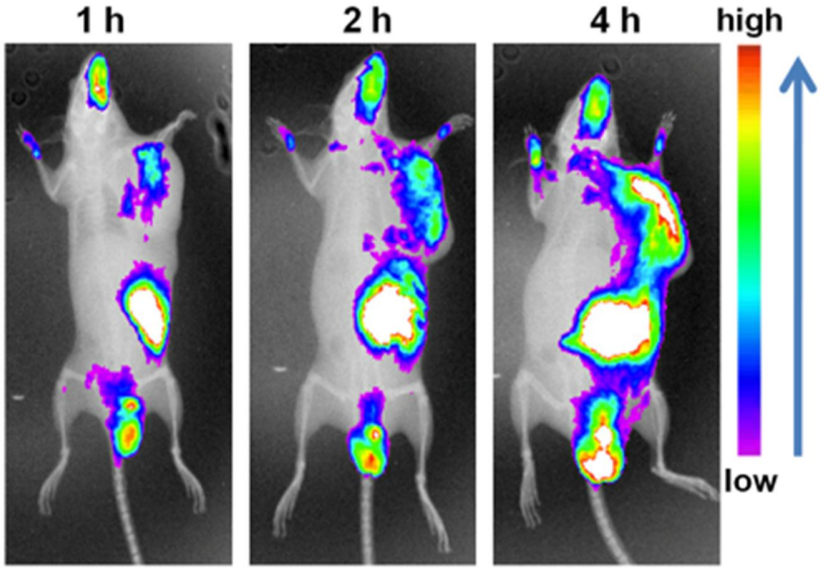

Figure 9